



Computational thermal analysis of a double slope solar still using Energy2D

José Andrés Alanís Navarro^{a,*}, Margarita Castillo Téllez^b, Mario Arturo Rivera Martínez^a, Gabriel Pedroza Silvar^a, Francisco Christian Martínez Tejada^a

^aCarretera federal Iguala-Taxco km 105, Puente Campuzano, Taxco de Alarcón – Guerrero, 40321, Mexico, Tel. +52(733)1029960, emails: aalanis@upeg.edu.mx (J.A.A. Navarro), mrivera@upeg.edu.mx (M.A.R. Martínez), gpedroza@upeg.edu.mx (G.P. Silvar), fcmat@ier.unam.mx (F.C.M. Tejada)

^bAv. Agustín Melgar, Buenavista, Campeche - Campeche, 24039, Mexico, Tel. +52(981)8119800, email: mcastill@uacam.mx

Received 28 June 2018; Accepted 20 January 2019

ABSTRACT

A theoretical evaluation of a double slope solar still using the Energy2D computer program is presented in this document. The heat absorbing plate is 0.25 m² square, 5 cm high and constructed of stainless steel. The water film is 3 cm high. Conduction heat losses of three commercial thermal insulation were studied: (i) polyurethane (PU), (ii) glass wool (GW), and (iii) expanded polystyrene (EPS). The insulation thickness is 15 cm and the glass cover is tilted at an angle of 30°. For the simulation, thermal conductivity, specific heat, mass density, and optical properties such as emittance, absorptance, reflectance, and transmittance coefficients were considered. After five hours of simulation, the left, central and right zones of insulator indicates 29.7°C; 45.2°C; 25.2°C, while the left, central and right zones indicates 75.7°C; 75.0°C; 75.5°C. The heat flux insulator, water and glass cover in its central zones are: 16.4, 301 and 72.9 W.m⁻², correspondingly. The lower heat loss was observed when PU is used as thermal insulation, while the greater loss when EPS is used. The three materials PU, EPS, and GW registered a temperature of 45°C, at a simulation time of 3 h, 1.5 h, and 45 min, respectively.

Keywords: Solar still; Solar desalination; Eco-technology; Heat transfer; Energy2D

1. Introduction

At present, the greatest challenge facing humanity is water supply. Increased demand, due to industrial development as well as demographic and economic growth limits its availability. The current energy circumstances require new technologies and environmental friendly methods to meet the most basic human needs in addition to enhancing the efficiency of existing systems. An important technology that contributes to a solution for a shortage of drinking water is distillation through solar thermal energy, or solar distillation. In order to develop this technology, it is necessary to understand the thermal-physical-chemical phenomena involved in the distillation process in order to optimize its efficiency. There are studies dealing with water desalination that provide basic information on solar energy desalination

methods, including small-capacity installations with practical applications, or used as demonstration pilot units [1]. Other research are based on configurations including single or double slopes, double deck cover, passive, and active stills [2], as well as multi-stages coupled to evacuated tube collectors [3,4]. Some solar still technologies have also been adapted to external parabolic reflectors [5]. In addition, the effects of the inclination of an external reflector attached to the still have been studied [6], as well solar collectors with a water storage tank [7]. There are theoretical studies on the effects of the cover, heat absorber and insulator on the productivity of a still [8] and expanded polystyrene [9]. Ghachem et al., [10] studied the effects of the buoyancy ratio and the angle of inclination to optimize the distiller that promotes maximum heat and mass transfer. As a result, it was determined that a

* Corresponding author.

buoyancy ratio with value of 1.5 and an inclination angle of -30° are the optimal parameters for the distiller. Al-Sulttani et al. [11] studied the performance of a new hybrid double-slope solar still with rubber scraper. As a result, it was observed that in the first one, more drops of water condensation are generated, which means that the productivity of water is 63% compared with the second. A theoretical study of the components determining the efficiency of a still is crucial to evaluate the influence of the operational and design parameters, as mathematical regression and linear modelling is used to accurately predict the productivity of a solar still ladder type [12]. El-Samadony et al. [13] presented a new theoretical analysis of heat radiation transfer rate inside a stepped solar still. They also reported the productivity of the solar still is found to be sensitive to the radiation shape, particularly at low solar insolation and/or high glass cover inclination angle and vice versa, obtaining an acceptable correlation with a maximum deviation of 3.16%. Furthermore, exergetic efficiency analysis of a passive solar still, including design, operational and climatic parameters has been studied [14], in addition to the exergy analysis of passive solar stills through the analysis of a single slope still [15] in which a theoretical exergy analysis is presented in the steady and transient states of the main components of a solar still, as well as the ergonomic optimization of a solar distillation system in order to evaluate the parameter costs, together with the energy and exergy system analysis [16]. Dumka and Mishra [17] evaluated solar-earth water still suitability, analyzing the energy and exergy of a modified single slope solar still integrated with earth and conventional single slope. As a result they observed an increase in efficiency, energy and exergy. Another important aspect is the computational modelling and simulation in order to improve the still's performance. This can be done by using a multi-phase computational fluid dynamics model in simulation software such as Ansys Fluent, checking the correspondence between the experimental and simulated data [18]. Likewise, Alvarado-Juárez et al. [19] reported the numerical study of double-diffusive natural convection in a tilted rectangular cavity. The study analyzes the effect of the glass cover in the aspect ratio range of $5 \leq A \leq 20$, and in the tilt angle interval $15^\circ \leq \theta \leq 35^\circ$. They conclude that when aspect ratio decreases, the multicell pattern decreases, and the convective heat and mass transfer increase up to 41%. As the tilt angle increases, the Sherwood and Nusselt numbers increase up to 3.8% and the condensate of water increases about 3% when the one-cell pattern prevails. On the other hand, Maalem et al. [20] established a model of heat and mass transfer phenomena in a trapezoidal cavity. This study was partly based on experimental results obtained in the case of a trapezoidal-shaped solar distiller.

In this study, a theoretical evaluation of a double slope solar still using the Energy2D software is performed. This computer-aided engineering free software has been previously used by [21,22,23], and widely recommended in [24]. The still consists of a simple thermally insulated base, heat radiation stainless steel absorber of 0.25 m^2 and 5 cm high, which also has the function of containing the water to be distilled. The water film to be distilled is 3 cm in depth. Three commercial thermal insulation materials are studied: (i) polyurethane, PU; (ii) glass wool, GW; and (iii) expanded

polystyrene, EPS. The thickness of the insulation is 15 cm. For the simulation, thermal conductivity, specific heat, mass density, and optical properties such as emissivity, absorption, reflection and transmission coefficients are evaluated. The study consists of a non-stationary heat transfer simulation of a double slope solar still, and the influence of several thermal insulators on the temperature and heat flux distribution over different still components.

2. Materials and methods

The criterion for selection of solar still includes economic aspects, availability and easy access to the material for its construction. The system that fulfils these requirements is the single-base still or simple-base, passive, cooled by natural convection [8]. By not using forced convection, the use of fans and their respective energy supply system is avoided, although it may consist of a photovoltaic system for the supply of electric energy, even though this implies an additional cost. The analyzed prototype uses glass as a cover, polyurethane as the insulating material, a stainless-steel tray as a heat absorber and container of water to be distilled, and polyvinyl-chloride (PVC) pipes, which are easily accessible and inexpensive. Being a prototype, the physical dimensions were chosen to provide portability as did previous studies [1]. A comparison of three commercial thermal insulators includes: polyurethane, glass wool and expanded polystyrene. The parameter that allows them to be compared to each other is their thermal conductivity. Although, the three materials have similar conductivity, in practice, EPS continues to be used, mainly for its low cost, while glass wool has the disadvantage of absorbing water [25]. The still consists of the following components: (i) a stainless steel heat absorber of 5 mm thickness, 50×50 cm base, 5 cm high; (ii) thermal insulator of 80×80 cm base and 15 cm high; (iii) a glass cover 15 cm high and 4 mm of thickness, this allows the cover to have 30° tilt; and (iv) a water film to be distilled 3 cm in depth. This study consists in the simulation of the heating and cooling process of the device by using commercial and free access computational software. The temporal variation of the temperature (T) and the heat flux (q'') is obtained in different zones: left (l), central (c), right (r), upper (u); of polyurethane (p), water (w), and glass (g).

2.1. Simulation in Energy2D

For the development of the simulation, a free-access general purpose computer program called Energy2D or computer-aided engineering (CAE) system from the Concord consortium [26] is used to simulate the heat transfer phenomena in two dimensions, and at a non-stationary state. The first step to simulate the thermal performance, is to define the medium properties such as background temperature, thermal conductivity, specific heat, mass density, viscosity, etc. In Energy2D, this must be done in the *Model Properties* menu (Fig. 1(a)). If solar radiation needs to be taken into account, it must be activated in the *Sunlight*, sub-menu. Thermal and mass boundary conditions can be established in the *Boundary* sub-menu of the *Model Properties* menu, (Fig. 1 (b)). Upper, right, lower

2.2. Temperature and heat flux sensors

The temperature sensors of the insulator are identified by the following nomenclature: T_{il} is used to distinguish the temperature sensor located on the left side of the thermal insulation, T_{ic} for the central zone sensor, and T_{ir} for the right-side zone; analogously for the sensors placed on the glass cover: T_{gl} , T_{gc} and T_{gr} for left, center and right sensors, respectively. The thermal properties of each element considered in the simulation are presented in Table 1, namely: thermal conductivity, λ ; specific heat, c_p ; mass density, ρ_m ; also the main optical properties were considered, these are: emissivity or emittance, ε ; absorption or absorptance, α ; reflection or reflectance, ρ ; and transmission or transmittance, τ .

In a similar way, sensors available in Energy2D software are used for heat flux quantification. The heat flux sensors of the insulator are identified by the following nomenclature: q''_{il} is used to distinguish the heat flux –by conduction– sensor located on the left side of the thermal insulator; q''_{ic} for the sensor of the central zone, and q''_{ir} for the right side; in a similar manner for the heat flux sensors placed on the double deck glass cover: q''_{gl} , q''_{gc} and q''_{gr} for left, center and right side heat flux sensors, respectively. The precise location of each heat flux sensor is presented in Appendix (Fig. A1).

3. Results and discussion

A series of simulations under different conditions were performed to analyze the heat transfer from the heat absorbing plate to the water film, as well the heat losses by conduction from the stainless-steel plate to the insulator material. The heating process was evaluated and compared using three commercial materials as the insulating component: (i) polyurethane (PU), (ii) glass wool (GW), and (iii) expanded polystyrene (EPS). Natural convection heat losses from the water film into the glass shell and from the glass to the environment were also evaluated. Once the best insulating material was identified, the cooling process simulation was performed, analyzing and comparing different zones, principal heat flux, and temperature sensors. For all simulations the initial and boundary thermal conditions were established. The initial and boundary thermal conditions are Dirichlet type, i.e., constant

temperature [32]. The stainless-steel heat absorber was set at 80°C, also known – in Energy2D software – as *Constant temperature*, while surroundings were set an environmental temperature of 20°C, including the insulating material, the water film, the glass cover and the surrounding inner air. However, excepting the heat absorbing plate, all the materials can increase or decrease its temperature as time increases, also known in Energy2D software as *not a heat source*, due to the aforementioned heat transfer mechanisms. Once heating process simulation is done, the opposite procedure is simulated, i.e., the cooling process, but only by natural convection. The maximum steady-state values of each component during heating simulation, was considered as the initial value for the cooling process simulation. The temperature-time evolution in different zones of the thermal insulator, on water film and over the glass cover, was obtained. Also, the temporal changes of the heat flux observed at the same points where the temperature was measured, allowing a comparison between both analyzed variables. The simulation time is a function of the acquired value by the temperature and heat flux variables, either by conduction or by natural convection. The stop criterion of each simulation is the point where there was no change in the value of measured variables.

3.1. Heating process: temperature and heat flux distribution

The temperature distribution on the heat absorbing plate, on the water film, and the insulator is shown in Fig. 4. This figure also notes the streamline under and over the double slope glass cover. The color bar at the top of the figure represents the magnitude of the temperature. The blue color corresponds to 20°C, while the white one is associated with the highest temperature, i.e., 80°C, corresponding to the stainless-steel heat absorbing plate. Likewise, the red and yellow colors correspond to a temperature of 40°C and 60°C, respectively. In this simulation, the rest of the elements, including the air surrounding the design were set at 20°C and to be in thermal equilibrium. Basically, the heat transfer involves the thermal conduction through stainless steel and water film, from stainless steel to insulator, natural convection through water film and inner air of the glass cover, heat conduction in the glass cover, and finally, natural convection from insulator and glass cover to the environment. The influence of three commercial insulating materials: PU, GW, and EPS, was analyzed via a

Table 1 Thermal properties of solar still components. Source: Own elaboration with information of [27], [28], [29], [30], [31]

Material	Property		
	ρ_m ($\text{kg}\cdot\text{m}^{-3}$)	λ ($\text{W}\cdot\text{m}^{-1}\cdot^\circ\text{C}^{-1}$)	C_p ($\text{J}\cdot\text{kg}^{-1}\cdot^\circ\text{C}^{-1}$)
Air	12	0.026	1,005
EPS	16	0.040	1,200
Glass	2,600	0.960	840
GW	66	0.039	670
H ₂ O _(l)	998	0.600	4,182
PU	70	0.026	1,045
Steel	7,913	15.60	456

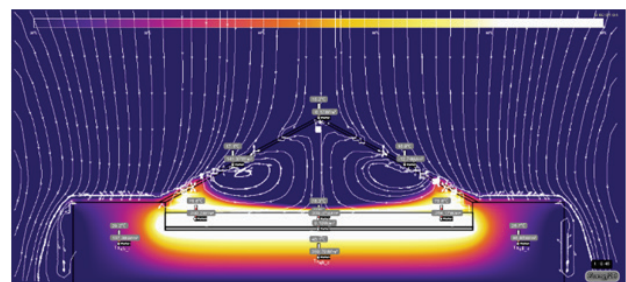


Fig. 4. Streamlines over the double slope glass cover and temperature distribution on the absorbing plate, water film and insulator.

2D non-stationary simulation by comparing the temperature using the T_{ic} sensor (see Fig. 5). A slower temperature increase when PU is used was observed, but when EPS was used, a rapid increasing in temperature was observed, reaching 40°C in less than one-half-hour, and when PU was used, the same temperature was reached after an hour and forty-five minutes, approximately. A similar analysis was performed to compare another zone of insulating material. In this case, the temperature was evaluated at the left lateral zone, using T_{il} sensor, for the same insulating materials. The results are presented in Fig. 6.

Fig. 7 demonstrates the overall temperature distribution of the solar still after one half hour simulation. Heat transfer – by conduction – through the insulator is clearly observed, as well as the water heating process, by means of heat conducting from the stainless-steel heat absorbing plate. The obtained temperature and heat flux variation vs. time over the central zone of insulator are shown in Fig. 8. There is a rapid increase in heat flux during the first one half hour, followed by a slow change in heat flux, reaching nearly 360 W·m⁻². On the other hand, temperature vs. time of the central zone of the water film is shown in Fig. 9. A heat flux peak is depicted in about the first twenty minutes of simulation, followed by a rapid increase in the roof’s temperature, causing additional heat losses from the cover, this can be seen in Fig. 10(a). After five hours of simulation, the sensors T_{il} , T_{ic} , T_{ir} , T_{wlr} , T_{wlc} , T_{wr} and T_{gc}

registered 29.7°C; 45.2°C; 25.2°C, 75.7°C; 75.0°C; 75.5°C and 11.7°C, respectively, while the sensors q''_{ic} , q''_{wc} and q''_{gc} registered 16.4, 301.7, and 72.9 W·m⁻², correspondingly.

Once upon the water film has reached a thermal equilibrium with respect to the absorbing plate, the double deck glass cover is heated by the surrounding air (Fig. 10(a)). Convective heat losses to the environment are shown in Fig. 10 (b). The changes over time of the temperature of the insulating and glass cover at several zones, is shown Fig. 11, while temperature and heat flux variation on the central zone of the double slope glass cover is presented in Fig. 12.

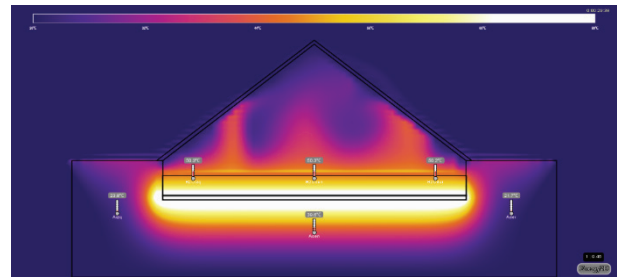


Fig. 7. Temperature distribution on the absorbing plate, thermal insulator and on the water film.

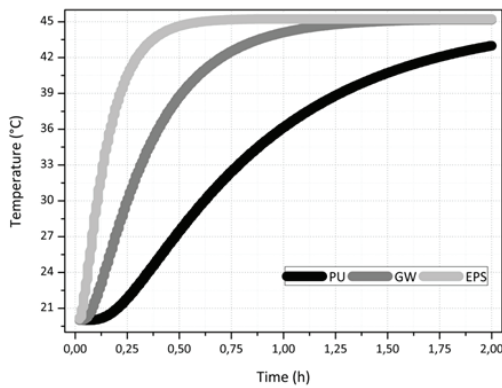


Fig. 5. Temperature vs. time of insulator measured through T_{ic} sensor, of the three studied insulator materials.

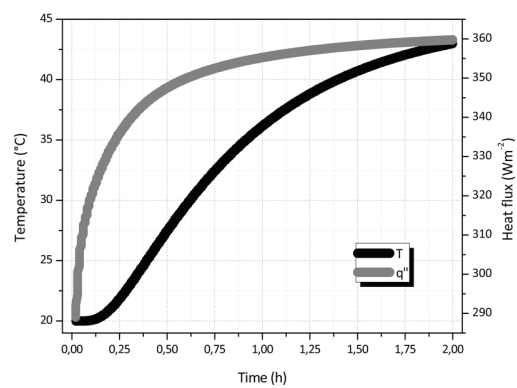


Fig. 8. Temperature and heat flux vs. time of T_{ic} sensor.

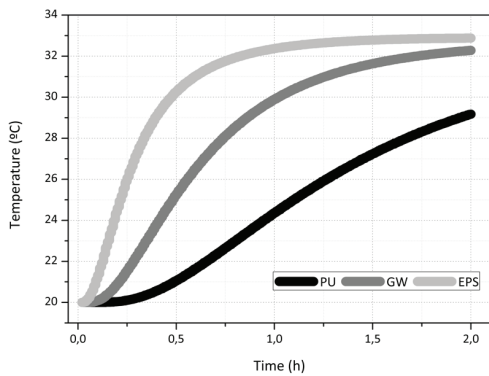


Fig. 6. Temperature vs. time measured through sensor T_{il} of the three studied insulation materials.

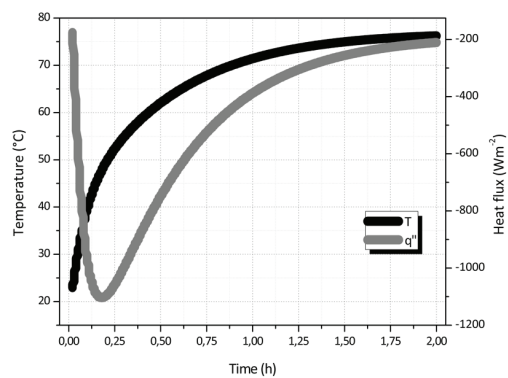


Fig. 9. Temperature and heat flux vs. time of T_{wlc} sensor.

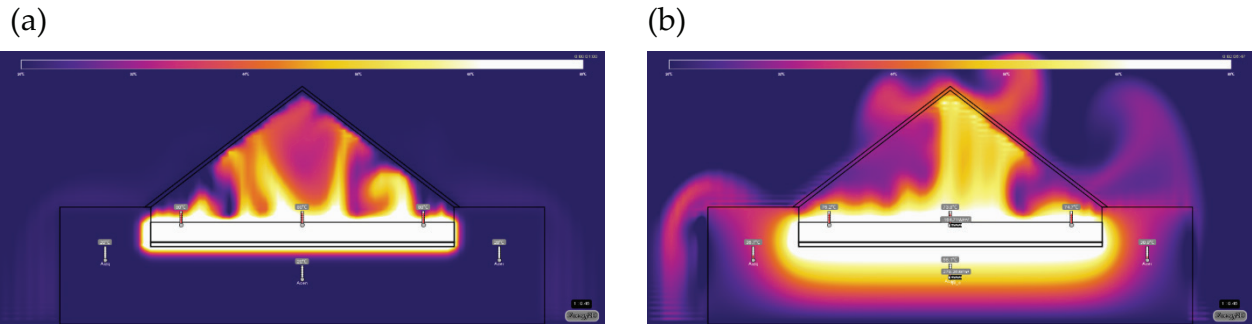


Fig. 10. Temperature distribution inside the double slope glass cover (a) and outside the glass cover (b).

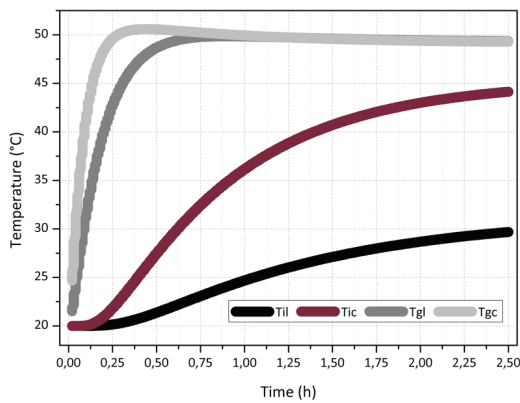


Fig. 11. Temperature vs. time over the thermal insulator and double slope glass cover in several zones.

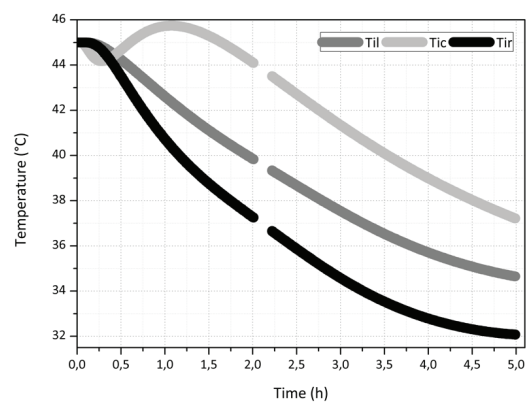


Fig. 13. Cooling process over three zones of polyurethane.

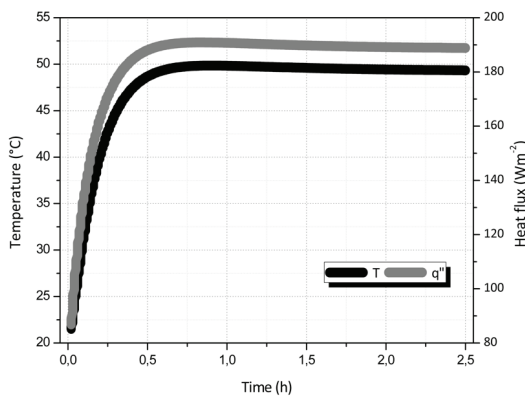


Fig. 12. Temperature and heat flux versus time on the central zone of the double slope glass cover.

3.2. Cooling process: natural convection

For the cooling process, the maximum values at steady-state during the heating process were set as the initial conditions. Insulator temperature, water film and glass cover were set at 45°C, 75°C and 63°C, respectively, while the environmental temperature was set at 28°C, based on the average local environmental temperature at middle day, measured by using a meteorological system. After 5 h of simulating the cooling process – by natural convection - temperature sensors T_{il} , T_{ic} , T_{ir} , T_{wl} , T_{wc} , T_{wr} and T_{gc}

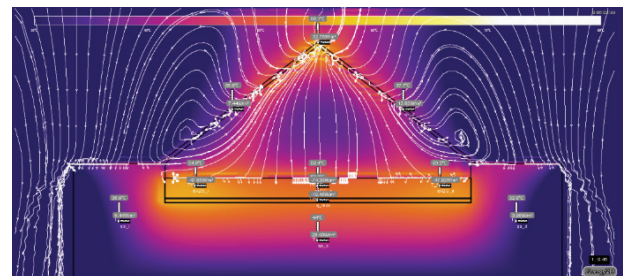


Fig. 14. Streamlines and temperature distribution during the cooling process.

registered: 34.7°C; 37.3°C; 32.8°C, 44.1°C; 43.4°C; 43.9°C and 31.5°C, respectively, whereas the heat flux sensor q''_{ic} , q''_{wc} and q''_{gc} registered: 74.4, 53.8 and 17.6 W·m⁻², separately. The changes of the PU's temperature during this process is shown in Fig. 13. After two hours simulation a gap in the data is observed, because of the internal storage limit of the Energy2D software, but simulation was restarted to show more detailed cooling process graphs. The streamlines and temperature distribution after the aforementioned simulation time is depicted in Fig. 14.

4. Conclusions

A Double slope solar still evaluation by simulation using the Energy2D computer-aided engineering system was conducted. Using Dirichlet type thermal boundary

condition, non-stationary simulations were performed under different conditions and considering the most important thermal and optical properties. Streamlines, temperature and heat flux distribution representative figures over the solar still components are shown. Heat losses were compared by using three commercial insulating materials: polyurethane, glass wool, and expanded polystyrene. These materials registered a temperature of 45°C, at the simulation time of 3 h, 1.5 h, and 45 min, respectively. The best insulating material was polyurethane, while the worst was expanded polystyrene. For the cooling process, only natural convection was considered; the average temperature of all sensors located at polyurethane 34.9°C, while the water average temperature was 42.8°C. However, in future studies, additional forced-convection thermal analysis will be performed. Also, in a future study, the experimental evaluation and comparison with the theoretical simulated will be done and optimized.

Acknowledgments

Thanks to Professor María Belén Magadán Hernández for their support in English grammar and spelling corrections.

Symbols

c_p	–	Specific heat, $\text{J}\cdot\text{kg}^{-1}\cdot\text{C}^{-1}$
EPS	–	Expanded polystyrene
GW	–	Glass wool
PU	–	Polyurethane
PVC	–	Polyvinyl-chloride
q''_{ic}	–	Heat flux at central zone of insulator, $\text{W}\cdot\text{m}^{-2}$
q''_{il}	–	Heat flux at left zone of insulator, $\text{W}\cdot\text{m}^{-2}$
q''_{ir}	–	Heat flux at right zone of insulator, $\text{W}\cdot\text{m}^{-2}$
q''_{wi}	–	Heat flux at central zone of the water film, $\text{W}\cdot\text{m}^{-2}$
q''_{wl}	–	Heat flux at left zone of the water, $\text{W}\cdot\text{m}^{-2}$
q''_{wr}	–	Heat flux at right zone of the water film, $\text{W}\cdot\text{m}^{-2}$
T^{gc}	–	Temperature at central zone of the glass cover, °C
T^{gl}	–	Temperature at left zone of the glass cover, °C
T^{gr}	–	Temperature at right zone of the glass cover, °C
T_{ic}	–	Temperature at central zone of insulator, °C
T_{il}	–	Temperature at left zone of insulator, °C
T_{ir}	–	Temperature at right zone of insulator, °C
T_{wc}	–	Temperature at central zone of the water film, °C
T_{wl}	–	Temperature at left zone of the water film, °C
T_{wr}	–	Temperature at right zone of the water film, °C

Greek

α	–	Absorptance, 1
ε	–	Emittance, 1
λ	–	Thermal conductivity, $\text{W}\cdot\text{m}^{-1}\cdot\text{C}^{-1}$
ρ	–	Reflectance, 1
ρ_m	–	Mass density, $\text{kg}\cdot\text{m}^{-3}$
τ	–	Transmittance, 1

References

- [1] V. Belessiotis, S. Kalogirou, E. Delyannis, Thermal Solar Desalination: Methods and Systems, Elsevier, 2016.

- [2] G. Tiwari, L. Sahota, Review on the energy and economic efficiencies of passive and active solar distillation systems, Desalination, 401 (2017) 151–179.
- [3] K. Reddy, H. Sharon, Energy-environment-economic investigations on evacuated active multiple stage series on solar distillation unit for potable water production, Energy. Convers. Manage., 151 (2017) 259–285.
- [4] R.K. Lal, S.V.P. Yadav, J. Dwivedi, H. Dwivedi, Comparative performance evaluation of an active/passive solar distillation system, Materials. Today., 4 Part A (2017) 2822–2831.
- [5] H. Manchanda, M. Kumar, Performance analysis of single basin solar distillation cum drying unit with parabolic reflector, Desalination, 416 (2017) 1–9.
- [6] H. Tanaka, Y. Nakatake, Effect of inclination of external plate reflector of basin type still in winter, Solar Energy, 81 (2007) 1035–1042.
- [7] P. Kalita, S. Borah, D. Das, Design and performance evaluation of a novel solar distillation unit, Desalination, 416 (2017) 65–75.
- [8] S. Toure, P. Meukam, A numerical model and experimental investigation for a solar still in climatic conditions in Abidjan (Côte d'Ivoire), Renew. Energy., 11 (1997) 319–330.
- [9] C. Esteban, J. Franco, A. Paulo, Construction and performance of an assisted solar still, Desalination, 173 (2005) 249–255.
- [10] K. Ghachem, C. Maatki, L. Kolsi, N. Alshammari, H.F. Oztop, M.N. Borjini, K. Al-Salem, Numerical study of heat and mass transfer optimization in a 3D inclined solar distiller, Therm. Sci., 21 (2017) 2469–2480.
- [11] A.O. Al-Sulttani, A. Ahsan, A. Rahman, N.N. Daud, S. Idrus, Heat transfer coefficients and yield analysis of a double-slope solar still hybrid with rubber scrapers: an experimental and theoretical study, Desalination, 407 (2017) 61–74.
- [12] M.S.S. Abujazar, F. Suja, I.A. Ibrahim, A. Kabeel, S. Sharil, Productivity modelling of a developed inclined stepped solar still system based on actual performance and using a cascaded forward neural network model, J. Cleaner. Prod., 170 (2018) 147–159.
- [13] Y.A.F. El-Samadony, W.M. El-Maghlany, A.E. Kabeel, Influence of glass cover inclination angle on radiation heat transfer rate within stepped solar still, Desalination, 384 (2016) 68–77.
- [14] S. Kumar, G. Tiwari, Analytical expression for instantaneous exergy efficiency of a shallow basin passive solar still, Int. J. Therm. Sci., 50 (2011) 2543–2549.
- [15] J. Torchia-Nunez, M. Porta-Gandara, J. Cervantes-de Gortari, Exergy analysis of a passive solar still, Renew. Energy., 33 (2008) 608–616.
- [16] A.G. Ibrahim, A.M. Rashad, I. Dincer, Exergoeconomic analysis for cost optimization of a solar distillation system, Solar. Energy., 151 (2017) 22–32.
- [17] P. Dumka, D.R. Mishra, Energy and exergy analysis of conventional and modified solar still integrated with sand bed earth: study of heat and mass transfer, Desalination, 437 (2018) 15–25.
- [18] V.R. Khare, A.P. Singh, H. Kumar, R. Khatri, Modelling and performance enhancement of single slope solar still using CFD, Energy. Procedia., 109 (2017) 447–455.
- [19] R. Alvarado-Juárez, J. Xamán, G. Álvarez, I. Hernández-López, Numerical study of heat and mass transfer in a solar still device: effect of the glass cover, Desalination, 359 (2015) 200–211.
- [20] M.S. Maalem, A. Benzaoui, A. Bouhenna, Modeling of simultaneous transfers of heat and mass in a trapezoidal solar distiller, Desalination, 344 (2014) 371–382.
- [21] M. Abderrezek, M. Fathi, Experimental study of the dust effect on photovoltaic panels' energy yield, Solar. Energy., 142 (2017) 308–320.
- [22] W. Punin, S. Maneewan, C. Punlek, Heat transfer characteristics of a thermoelectric power generator system for low-grade waste heat recovery from the sugar industry, Heat Mass Transfer, 2018, doi.org/10.1007/s00231-018-2481-5. Available at: <https://link.springer.com/article/10.1007/s00231-018-2481-5>.
- [23] A. Massaro, A. Galiano, G. Meuli, S.F. Massari, Overview and application of enabling technologies oriented on energy routing monitoring, on network installation and on predictive maintenance, Int. J. Artif. Intell. Applic., 9 (2018) 1–20.

- [24] J. Tu, G.H. Yeoh, C. Liu, *CFD Solution Procedure: A Beginning, Computational Fluid Dynamics: A Practical Approach*, Butterworth-Heinemann, Elsevier, 2018, pp. 33–62.
- [25] I.I. Marhoon, A.K. Rasheed, Mechanical and physical properties of glass wool-rigid polyurethane foam composites, *Al-Nahrain J. Eng. Sci.*, 18 (2015) 41–49.
- [26] C. Xie, *Energy2D Interactive Heat Transfer Simulations for Everyone*, 25 10 2018. [En línea]. Available at <http://energy.concord.org/energy2d/>.
- [27] T.L. Bergman, F.P. Incropera, D.P. DeWitt, A.S. Lavine, *Fundamentals of Heat and Mass Transfer*, John Wiley & Sons, 2011.
- [28] W.M. Haynes, *CRC Handbook of Chemistry and Physics*, CRC Press, 2014.
- [29] Engineering ToolBox, 15 10 2018a [En línea]. Available at http://www.engineeringtoolbox.com/density-materials-d_1652.html.
- [30] Engineering ToolBox, 15 10 2018b [En línea]. Available at http://www.engineeringtoolbox.com/specific-heat-capacity-d_391.html.
- [31] Engineering ToolBox, 15 10 2018c [En línea]. Available at: http://www.engineeringtoolbox.com/thermal-conductivity-d_429.html.
- [32] Y. Bazilevs, T.J. Hughes, Weak imposition of dirichlet boundary conditions in fluid mechanics, *Computers. Fluids.*, 36 (2007) 12–26.
- [33] S. Sharshir, A. Elsheikh, G. Peng, N. Yang, M. El-Samadony, A. Kabeel, Thermal performance and exergy analysis of solar stills a review, *Renew. Sustain. Energy. Rev.*, 73 (2017) 521–544.

Appendix

Heat flux sensors location

The exact location of each flux sensor is presented in Fig. A1.

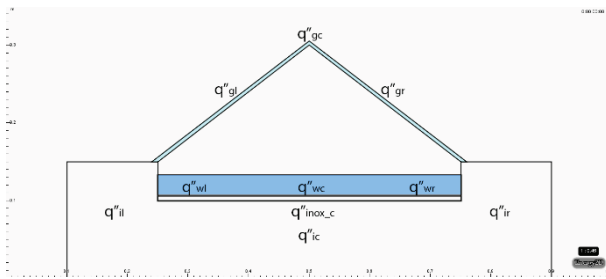


Fig. A1. Heat flux sensor location.